

# Measuring the electron electric dipole moment in YbF

B. E. Sauer, J. J. Hudson, M. R. Tarbutt, E. A. Hinds

*Sussex Centre for Optical and Atomic Physics, University of Sussex,  
Falmer, Brighton BN1 9QH, UK*

**Abstract.** We describe the current status of the experiment at Sussex to measure the electron's permanent electric dipole moment  $d_e$  using the paramagnetic molecule YbF. We consider a number of systematic effects which could mimic  $d_e$  and conclude that they are far below the current experimental sensitivity. As of June 2001 we have accumulated over 20 hours of data, which combined give a measurement  $d_e = 0.6 \pm 4 \times 10^{-26}$  e.cm.

## INTRODUCTION

For over half a century, it has been recognised that an elementary particle cannot have a permanent electric dipole moment (edm) unless the discrete symmetries parity (P) and time reversal (T) are broken [1]. Since the early 1950's measurements have been made on a variety of elementary particles, atoms and molecules, all with null results suggesting that T violation is not exhibited in ordinary matter [2,3]. T violation does occur within the standard model of elementary particle physics through complex Yukawa couplings between the quarks (the KM mechanism [4]), indeed, this seems to explain the well-known CP-violating behaviour of kaons [5], but the edms predicted for ordinary matter are extremely small. This makes edm measurements very powerful in the search for new physics since any nonzero result immediately implies physics beyond the standard model [6,7].

## PRINCIPLE OF THE EXPERIMENT

The electron edm's interaction with a total electric field  $\mathbf{E}$  is described by the effective Hamiltonian  $H_{E1} = -d_e(\mathbf{1} - \beta)\boldsymbol{\Sigma} \cdot \mathbf{E}$ , where  $\beta$  and  $\boldsymbol{\Sigma}$  are standard Dirac matrices and the weak magnetic interaction is ignored (see §4 of [8] or §III of [9]). The explicit form of the interaction makes it clear that the effect is relativistic,

$$\langle H_{E1} \rangle = \langle \Psi_0 | \begin{array}{cc} 0 & 0 \\ 0 & 2d_e \boldsymbol{\sigma} \cdot \mathbf{E} \end{array} | \Psi_0 \rangle,$$

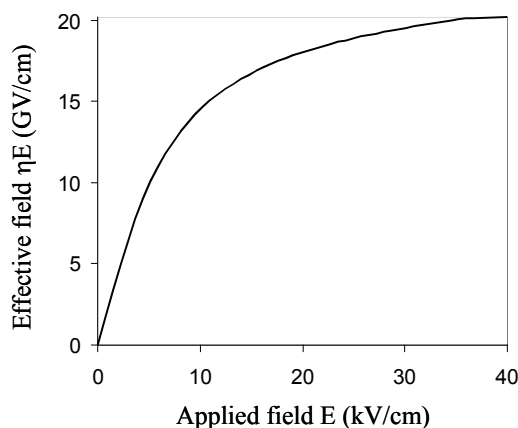


**FIGURE 1.** The effective field seen by the electron spin in YbF as a function of the applied lab field. Note the different scales, the enhancement  $\eta$  is about  $10^6$ . The asymptotic value of the effective field is calculated to be 26 GV/cm [11]. The current experiment at Sussex applies a field of 8kV/cm, which gives about half of the maximum effective field. The form of the curve,  $\langle \hat{\sigma} \cdot \hat{\lambda} \rangle$ , is that of the polarization of a rigid rotor.

as only the small components of the Dirac wavefunction  $\psi_0$  are important. The effect is therefore large in heavy atoms or molecules- an external electric field  $E_{ext} \hat{\lambda}$  can polarize the wavefunction near the heavy nucleus, yielding an energy  $\langle H_{E1} \rangle = d_e \eta E_{ext} \hat{\sigma} \cdot \hat{\lambda}$  ( $\hat{\sigma}$  is a vector along the electron's spin). As  $\hat{\lambda}$  is a polar vector this interaction clearly violates both P and T symmetry. Sandars [10] was the first to note that the effective field  $\eta E_{ext}$  is much larger than the applied field for heavy atoms. Recent calculations of the enhancement factor for a large number of atoms and molecules have been summarized by Commins [9]. A few years after Sandars discovered the atomic enhancement he also pointed out that heavy polar molecules, being far more polarizable than atoms, have a great advantage over atoms in that  $\eta E_{ext}$  can actually saturate in quite modest laboratory fields [11]. We have chosen YbF for our edm experiment as it is experimentally the most tractable of the simple heavy polar molecules. The polarization of YbF is shown in figure 1, where the asymptotic value of  $\eta E_{ext}$  has been calculated using several different methods to be about 26 GV/cm [12].

YbF has a simple hyperfine structure in the ground electronic, rotational and vibrational state used by the edm experiment. The electron spin and the  $I = \frac{1}{2}$  fluorine nuclear spin combine to produce an  $F=1$  triplet and an  $F=0$  singlet, separated by about 170 MHz. An applied electric field lifts the degeneracy between the  $|F, m_F\rangle = |10\rangle$  and the  $|1\pm 1\rangle$  states, although T symmetry requires that the  $|11\rangle$  and  $|1-1\rangle$  states remain degenerate, as shown in figure 2.

A magnetic field  $\vec{B}$  lifts this degeneracy by producing an energy shift  $-\mu_B \hat{\sigma} \cdot \vec{B}$  dependent on the direction of the electron spin ( $\mu_B$  is the electron's magnetic moment). In a P- and T-violating analogue of this, the edm interaction  $-d_e \hat{\sigma} \cdot \eta \vec{E}_{ext}$

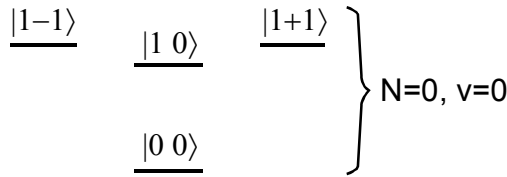


**FIGURE 2.** The hyperfine levels of the ground electronic, vibrational and rotational state of YbF (The rotational quantum number is  $N$ ). The  $F=1$  to  $F=0$  splitting is about 170MHz; the tensor splitting in the  $F=1$  manifold is shown in detail in figure 5.

also induces a level splitting which is what we seek to measure. This shift is of course very small and not accessible by normal spectroscopy. The Sussex YbF experiment therefore use an interferometric technique, illustrated in figure 3. We start by preparing a superposition state of two hyperfine levels  $\frac{1}{\sqrt{2}}(|11\rangle + |1-1\rangle)$ . When this state evolves for a time  $T$  in combined electric and magnetic fields, the two parts of the wavefunction develop a relative phase shift  $2\varphi = 2(d_e \eta E_{ext} + \mu_B B)T / \hbar$ . Probing the state in a way sensitive to this phase gives a signal proportional to  $\cos^2 \varphi$ ; by setting the magnetic phase to be  $\pi/4$  we maximize the edm signal produced when  $E$  is reversed relative to  $B$ .

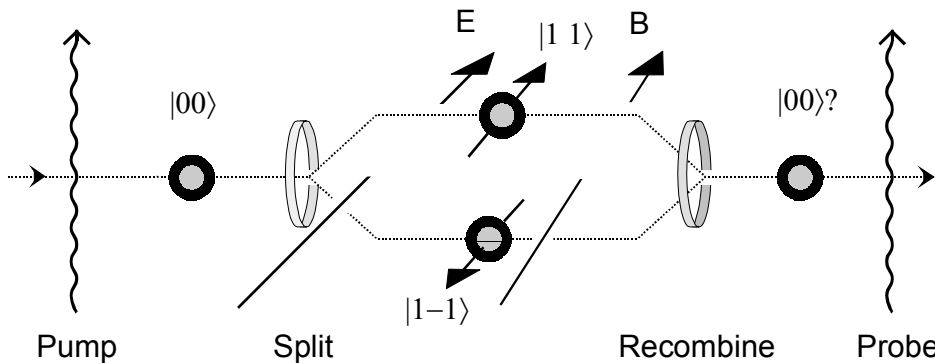


**FIGURE 3.** A schematic of the spin interferometer. The splitter and recombiner are driven by separate rf sources which have no mutual phase coherence.

## EXPERIMENTAL DETAILS

### The YbF apparatus

The YbF molecular beam is enclosed in an outer layer of magnetic shielding about 1.4 m long. YbF is produced by the reaction of Yb metal with  $AlF_3$  in a Mo crucible heated to 1500K. The resulting thermal beam has a most probable velocity  $v$  of  $440 \text{ ms}^{-1}$ . The YbF molecules first interact with  $\sim 552 \text{ nm}$  laser light tuned to the electronic transition  $P_{12}(2)$  exciting the  $F=1$  and  $F=2$  states of the  $N=2$  rotational

manifold and transferring the population by spontaneous decay to the ground state  $N=0$  shown in figure 2. A second laser beam tuned to the  $Q(0) F=1$  transition partially overlaps the first, this transfers population out of the ground state  $F=1$  manifold [13]. Two independent dye lasers are required to generate this light; their relative frequencies are stabilized via an external cavity lock. To the extent that the electronic transitions conserve the vibrational state this is a closed system, unfortunately the Franck-Condon factors for YbF have not been carefully measured but the vibrational leakage is expected to be small. The net effect of the laser transitions is to transfer molecular population to the  $|00\rangle$  state and to leave the  $F=1$  triplet unpopulated. The beam then enters an inner cylindrical magnetic shield which encloses the electric and magnetic interaction region.

The electric fields are produced by three pairs of plates, two short guard regions at either end and a  $\sim 60$  cm high field region. The plates are formed from 1.5mm aluminum sheet which was cut to size, electropolished and glued to glass backing plates. The backing plates are separated by precision glass spacers- the electrode spacing is uniform to 25  $\mu\text{m}$ . This arrangement has the advantage that it proved very easy to produce a uniform electric field region, unfortunately the presence of the glass dielectric limits the peak field in the center region to 8.3 kV/cm, which in turn limits the effective electric field to about half of its maximum value (figure 1). Referring to figure 3, the ‘splitter’ and ‘recombiner’ of the interferometer are rf loops which drive M1  $\pi$ -flip transitions between  $|00\rangle$  and the coupled state  $\frac{1}{\sqrt{2}}(|11\rangle + |1-1\rangle)$  in the  $\sim 3.3$  kV/cm guard fields. A magnetic field parallel to the electric field is produced by 4 wires glued to the inside of the inner magnetic shield at locations which produce a  $B_z$  field uniform to 1% across the beam [14].

After the YbF molecules leave the inner magnetic shield the population of the  $|00\rangle$  state is probed by collecting laser induced fluorescence from the  $F=0$  part of the  $Q(0)$  transition. The interference curve as a function of  $B_z$  is shown in figure 4. Note that the depth of the interference is only about 1% of the total count rate; the large background is caused by oven blackbody light, by scattered probe laser light and by overlapping molecular transitions.

As noted previously, the interferometer is most sensitive to small changes in phase when the magnetic field  $B_{z0}$  is set to the steepest point on either side of the central interferometer fringe. During data acquisition the slope of the curve at this point is measured by applying a small step in magnetic field. We record the fluorescence at eight points  $(\pm E_z, \pm(B_{z0} \pm \delta B_z))$  and take appropriate combinations to extract the edm, which is odd in  $\vec{E} \cdot \vec{B}$ , the slope, and various other diagnostic signals. As the applied magnetic fields are well characterized the experiment essentially measures the ratio  $d_e / \mu_B$ . A typical block of data consists of 1024 points where each point is measured for 50ms; the duty cycle per block is 65%, since additional time is added between points to allow switching transients to die away. The fields are switched using patterns which reject low frequency noise [15].

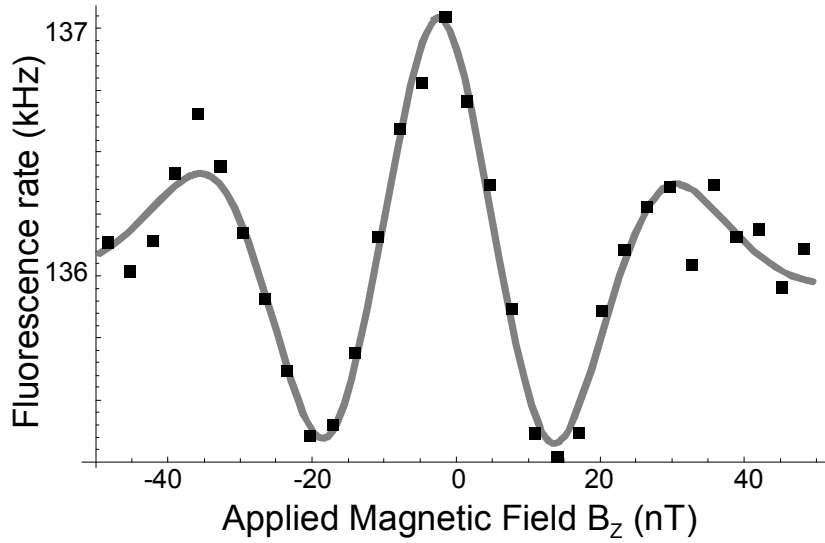


**FIGURE 4.**  $F = 0$  probe fluorescence signal rate (kHz) vs. applied  $B_z$  in the interference region. Each point represents 12s of integration time. The curve is a velocity averaged calculation whose only free parameters are the overall normalization and a magnetic field offset.

## SYSTEMATIC EFFECTS

Stray magnetic fields are a problem in all edm experiments because the electron's magnetic dipole moment  $\mu_B$  is so much larger than the edm  $d_e$  one hopes to measure. In general the YbF experiment is less sensitive than atomic experiments to stray magnetic fields because the enhancement of T violating effects is larger. In other words, the ratio  $\mu_B B_{stray} / d_e \eta E_{ext}$  is smaller because  $\eta$  is larger by roughly three orders of magnitude. Any magnetic field which reverses with the applied E field is dangerous; some well known effects are B fields due to leakage currents from the high voltage plates and the magnetic field generated by the motion of the molecules through the applied E field, which we discuss next.

### *The $\mathbf{E} \times \mathbf{v}/c^2$ motional magnetic field*

A polar molecule like YbF is highly anisotropic. Because it is strongly aligned along the direction of the applied electric field,  $\vec{E}_{ext}$ , which defines the  $z$  axis, it responds very differently to external fields parallel or perpendicular to  $\vec{E}_{ext}$ . This has the consequence that the edm signal is remarkably insensitive to transverse magnetic fields, in particular the motional field  $\vec{B}_E = \frac{\mathbf{v}}{c^2} E_{ext} \hat{x}$  which causes so much trouble in the Tl experiment. We estimate the size of this motional field effect for our

experiment as follows: (The same argument applies to transverse B fields generated by leakage currents.) Consider the effective Hamiltonian

$$\hat{H} = d_e \eta E_{ext} \hat{\sigma}_z + \mu_B B_{\parallel} \hat{\sigma}_z + \mu_B (B_{\perp} + B_E) \hat{\sigma}_x,$$

where the applied magnetic field makes an angle  $\alpha$  with  $E_{ext}$ , i.e.  $B_{\parallel} = B_{applied} \cos \alpha$ ,  $B_{\perp} = B_{applied} \sin \alpha$ . The edm signal is proportional to the energy difference  $U_{12}$  between the  $|11\rangle$  and  $|1-1\rangle$  states through the phase  $\varphi = \frac{1}{2} U_{12} T / \hbar$ . The lowest order term is diagonal in  $|F, m_F\rangle$  and picks out the parallel parts of the Hamiltonian,  $U_{12}^{(0)} = 2U_{\parallel} = 2(d_e \eta E_{ext} + \mu_B B_{\parallel})$ . The field  $\vec{E}_{ext}$  stark shifts the  $|10\rangle$  state by an energy  $\Delta$  relative to the  $|11\rangle$  state, as shown in figure 5. There is a second order mixing through this state with an energy given by

$$U^{(2)} = \frac{|\langle 1\pm 1 | \mu_B (B_{\perp} + B_E) \hat{\sigma}_x | 10 \rangle|^2}{E_{|1\pm 1\rangle} - E_{|10\rangle}} = \frac{|M|^2}{E_{|1\pm 1\rangle} - E_{|10\rangle}}.$$

The energy denominator is approximately  $\pm U_{\parallel} + \Delta$  which means that this second order shift is slightly different for the two states. The total energy difference is

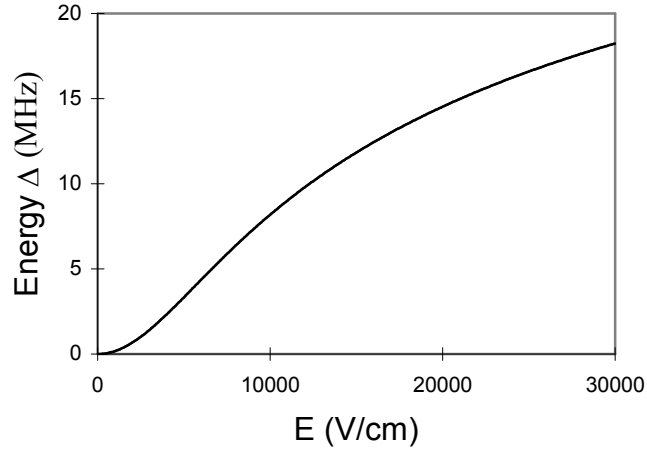


**FIGURE 5.** The energy splitting between the  $|11\rangle$  and  $|10\rangle$  hyperfine levels in an applied electric field.

$U_{12} = 2U_{\parallel} \left(1 - |M|^2 / \Delta^2\right)$ , to order  $|M|^2 / \Delta^2$ . Writing out the matrix element explicitly, we find there is a cross term  $\mu_B^2 B_{\perp} B_E$  which is potentially disastrous because it reverses with both  $E$  and  $B$ . However, it is strongly suppressed by the denominator  $\Delta^2$ , which is large because the molecule is very anisotropic and polarisable. If the applied  $E$  and  $B$  fields are exactly parallel there is no effect regardless of  $B_E$ , but even for large angles the systematic effect is strongly suppressed. For example, with a large misalignment of  $\alpha=10^\circ$  in our experiment, where  $B_{applied} \cong 200\mu\text{G}$ , this effect

produces only a small false edm of the order  $10^{-36}$  e.cm. In contrast to atomic experiments, where the energy levels usually respond to the magnitude of the total magnetic field, our interferometer scheme is exceptionally good at canceling this effect because it is sensitive to the energy *difference* between the  $|11\rangle$  and  $|1-1\rangle$  states, which are affected almost identically by perpendicular fields. This order of magnitude estimate is confirmed by numerically integrating the Schrödinger equation for the full wavefunction and the actual field distribution in the experiment. Also note that the systematics resulting from both the motional field and the leakage current fields will have functional dependencies on the applied  $E$  which are almost certain to be different to the true edm signal, which follows the form of the YbF polarization curve shown in figure 1.

### *Leakage currents*

Leakage currents from the high voltage plates which polarize the beam are a worry as they could produce a reversing magnetic field near the molecular beam. The  $z$  component couples to the electron's magnetic moment to mimic the edm whereas the transverse component is suppressed by the same mechanism that reduces the  $\mathbf{E} \times \mathbf{v}$  systematic. As a worse case estimate, a current which flows 1 cm from the beam produces an edm given by  $d_e[\text{e.cm}] < 10^{-19} I_{\text{leakage}}[\text{A}]$ , e.g. the leakage for our aluminium/glass plates  $I_{\text{leakage}} < 10\text{nA}$  gives a false edm of  $< 10^{-27}$  e.cm. In reality it seems unlikely that leakage currents are this effective at generating a false edm as there is not an obvious leakage path so close to the molecular beam which produces the correct orientation of magnetic field.

### *Intensity shifts*

So far, only one systematic effect has been significant. It results from change in beam intensity when the  $E$  field is reversed, together with an imperfect reversal of  $B$  due to slow drifts of the ambient magnetic field. The beam intensity change is due to a dependence of the RF "splitter" and "recombiner" transition efficiencies on the direction of the  $E$  field. We believe that the field does not reverse exactly, perhaps due to surface charges on the field plates or on nearby insulators. This inexact reversal leads to RF transition efficiencies that depend on the direction of  $E$ , through the Stark shift of the hyperfine levels. The inexactitude of the reversal, calculated from the size of the systematic edm, is around 5 V/cm. This is one of the reasons we are currently replacing the field generating electrodes.

On its own, this difference in RF efficiency is not enough to generate a false edm. However, in combination with a non-zero residual magnetic field inside the machine, a phoney edm results. The effect is best explained with reference to figure 6. The interferometer lineshape is rather crudely drawn, the solid and dashed lines represent the different RF efficiencies for the two directions of  $E$ . When we measure the edm,

the magnetic phase is set to  $\pi/4$  and the E field is reversed (points A and B). This is repeated with the magnetic phase set to  $-\pi/4$  (points C and D). The edm is proportional to  $(A + D - B - C)$ . Figure 6(a) shows the lineshape in the absence of any residual magnetic fields - the lineshape is centered on  $B_z = 0$ . Clearly in this case the false edm is zero, regardless of the RF efficiencies. Figure 6(b) shows the lineshape with the centre biased from zero. The edm,  $(A + D - B - C)$ , is no longer zero.

It is straightforward to extract both the difference in RF efficiencies for the two E directions and the residual  $B_z$  field from the data. The expected false edm can be calculated easily from these two quantities. This is then subtracted from the measured edm for that dataset to yield a corrected edm.

After the effect was discovered, we implemented a system to actively track the residual magnetic field, since if this field can be reduced to zero the effect disappears, provided that only the size and not the shape of the curve changes when E is reversed. During data acquisition the residual field is periodically calculated from the quantity  $(A + B - C - D)$  with recently acquired data. The strength of a canceling magnetic field is adjusted accordingly by a computer controlled current supply. With the magnetic field tracking active, the correction due to this intensity dependence is negligible.

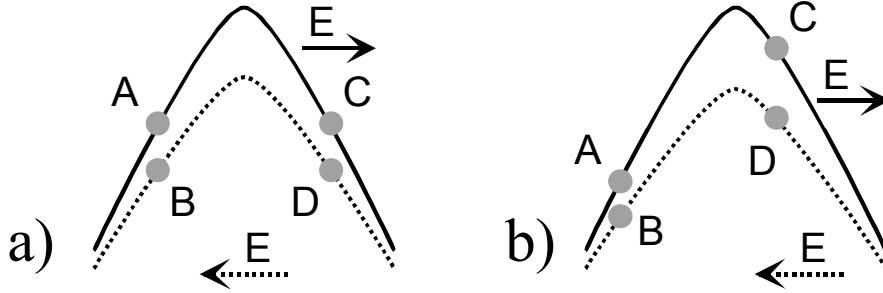


**FIGURE 6.** Simplified interferometer curves, showing points for the four combinations of  $(\pm E, \pm B_z)$  where data is acquired. A change in interferometer efficiency when E is reversed (solid/dashed lines), combined with a non-symmetric B reversal (b), gives a false edm. See text for details.

## RESULTS AND FUTURE PROSPECTS

We have accumulated about 23 hours of data with the current apparatus. The results are shown in figure 7; these data average to give a value of the edm  $d_e = 0.6 \pm 4 \times 10^{-26}$  e.cm, where the uncertainty is the  $1\sigma$  statistical error.

The limit to the precision of our measurement of  $d_e$  is entirely due to counting statistics. We are currently pursuing several possibilities which might increase the edm signal size and reduce the unwanted background. The electrodes for the electric field region will be replaced by a set with a new design. These new field plates are

aluminium coated with gold to reduce surface charging effects, which should reduce the problems associated with intensity shifts. The support structure for the plates has also been improved so that higher field strengths will be possible- we expect to reach ~80% polarization rather than 50%.

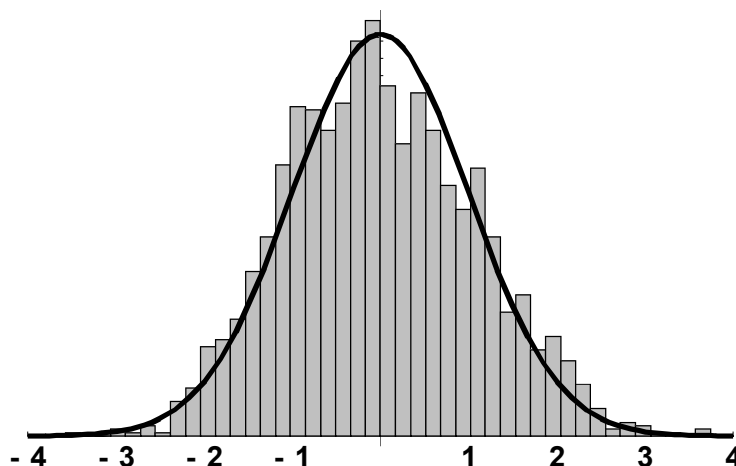


**FIGURE 7.** A histogram of our YbF edm data, where each 50s measurement has been normalized to its standard deviation. The curve is a Gaussian of unit width, centered on zero, whose overall height has been normalized to the data.

We have also begun to explore the possibility of producing a rotationally cold YbF beam. Our thermal source populates hundreds of rotational levels of the ground electronic state, so that only about  $10^{-4}$  of the YbF molecules which leave the oven are in the proper  $N=0$  state to participate in the edm experiment. It is a well established technique to produce rotationally cold refractory molecules by laser ablation of a suitable precursor into a gas whose expansion provides cooling. We are currently trying to implement this scheme for YbF. We have had preliminary success in producing YbF by ablating a solid target of  $\text{AlF}_3$  and Yb and are working towards a robust design for a laser ablation/supersonic expansion source. Success should increase the YbF experiment's sensitivity by two or three orders of magnitude.

## ACKNOWLEDGEMENTS

This work is supported by the UK research councils EPSRC and PPARC.

## REFERENCES

- 
1. E. M. Purcell and N. F. Ramsey, *Phys. Rev.* **78**, 807 (1950).
  2. I. B. Khriplovich and S. K. Lamoreaux, *CP violation without Strangeness*, (Springer Verlag, Berlin, 1996).
  3. For a review, see E. A. Hinds in *Atomic Physics 11*, (World Scientific Singapore 1989).
  4. M. Kobayashi and T. Maskawa, *Prog. of Theor. Phys.* **49** 652 (1972).
  5. *CP violation* edited by C. Jarlskog (World Scientific Singapore 1989).
  6. W. Bernreuther and M. Suzuki, *Rev. Mod. Phys.* **63** 313 (1991).
  7. S. M. Barr, *Int. J. Mod Phys. A* **8** 209 (1993).
  8. E. A. Hinds, *Physica Scripta*, **T70** 34 (1997).
  9. Eugene D. Commins, "Electric dipole moments of leptons", *Ad. At. Mol. Opt. Phys.* **40**, 1 (1999).
  10. P. G. H. Sandars, *Phys. Lett.* **14** 194 (1965).
  11. P. G. H. Sandars, *Phys. Rev. Lett.* **19**, 1396 (1967); The use of a polar molecule to search for  $d_e$  is implicit in this paper. The first explicit statement of the idea appears to be in O. P. Sushkov and V. V. Flambaum, *Zh. Eksp. Theo. Fiz* **75**, 1208 (1978) [*Sov. Phys. JETP* **48**, 608 (1978)].
  12. M. G. Kozlov, V.F. Ezhov, *Phys. Rev.* **A49** 4502 (1994); M. G. Kozlov, *J. Phys. B* **30** L607 (1997); A. Titov, M. Mosyagin, V. Ezhov, *Phys. Rev. Lett.* **77** 5346 (1996); H. M Quiney, H. Skaane, I. P. Grant, *J. Phys. B* **31** L85 (1998) (after correcting for the trivial factor of 2 between  $s$  and  $\sigma$  their result becomes 26 GV/cm); F. A. Parpia, *J. Phys. B* **31** 1409 (1998); N. Mosyagin, M. Kozlov, A. Titov, *J. Phys. B* **31** L763 (1998).
  13. B. E. Sauer, Jun Wang, E. A. Hinds, *J. Chem. Phys.* **105** 7412 (1996).
  14. G. D. Redgrave, D. Phil. Thesis, University of Sussex (1998), unpublished.
  15. M. A. Player and P. G. H. Sandars, *J. Phys. B* **3** 1620 (1970).